ORIGINAL ARTICLE

A reinforcement method of floor grouting in high-water pressure working face of coal mines: a case study in Luxi coal mine, North China

Minglei Zhai[1] · Haibo Bai[1] · Luyuan Wu[2] · Guangming Wu[3] · Xianzhen Yan[1] · Dan Ma[4]

Abstract
The working face is seriously threatened by limestone aquifer with high-water pressure in coal seam floor when Permo-Carboniferous coal is mined in North China Coalfield. Mine water control has become one of the major technical problems in coal mine production. Grouting transformation for limestone aquifer is an effective means to guarantee mining safety. A case of the 16,104 working face of the Luxi coal mine was studied in this paper. The results by the method of water-inrush coefficient (WIC) showed that there was a great risk of water inrush in 16,104 working face. There were differences between water-rich areas of floor aquifer obtained by geophysical methods and the areas with large water inflow by drilling exploration. The geophysical methods were performed again in the water-rich areas using traditional grouting method, results showed that the water-rich areas changed places, indicating that the effect of traditional grouting was not obvious. Grouting of areas of high-water inflow has reduced the water inflow. However, the grouting also has changed the water flow paths. What's more, the drill holes sealed poorly will also lead to the change of the position of the water-rich areas. To enhance overall grouting efficiency and cut down the repeated grouting times, a secondary grouting-reinforcement method was proposed to ensure amount grout injected into aquifer. The results showed that the grouting reinforcement was successful, which can provide reference for the treatment of floor confined water of North China Coalfield.

Keywords North China Coalfield · Floor water inrush · Geophysical methods · Grouting transformation · Drilling verification

Introduction

As a large coal-production country, the total output of raw coal for China was 3.85 billion tons in 2019, up 4% from the 2018. Although the proportion of coal in total energy consumption was 1.5% lower than 2018, still by more than 57 percent. The demand for coal will remain stable in the short term (Qian et al. 2018; Ma et al. 2021b).

✉ Dan Ma
dan.ma@cumt.edu.cn

1 State Key Laboratory of Geomechanics and Deep Underground Engineering, China University of Mining and Technology, Xuzhou 221116, Jiangsu, China

2 School of Civil Engineering and Architecture, Henan University, Kaifeng 475004, Henan, China

3 College of Civil Engineering, Ludong University, Yantai 264000, Shandong, China

4 School of Mines, China University of Mining and Technology, Xuzhou 221116, Jiangsu, China

North China is the main coal-producing area in China, and the coal fields is vast, stretching from the Qinlin mountains-Huai River in the south to Yinshan mountain in the north, and from the Yellow Sea in the east to the Helan mountain in the west (see Fig. 1), and the main coal seam is the Permo-Carboniferous coal (Hu et al. 2019a). Due to the influence of geological structure and other factors, many coal mines are endangered by water hazards from the Ordovician limestone (OL) aquifer (Dong et al. 2020; Guo et al. 2018; Wu et al. 2019; Shi et al. 2019a; Ma and Bai 2015; Ma et al. 2016; Hu et al. 2019b). To avoid water-inrush accidents in the floor of the working face, the grouting reinforcement of the floor aquifer is preferred to ensure mining safety above the confined aquifer (Sun et al. 2016; Yin et al. 2020; Dong et al. 2019; Cao et al. 2009).

The strength and elastic modulus of rock mass can be improved by grouting (Li et al. 2018a). To understand the grouting mechanism and effect of fractured rock mass, various scholars have carried out considerable research. For example, the formula for calculating the thickness of

Fig. 1 Location of the study area
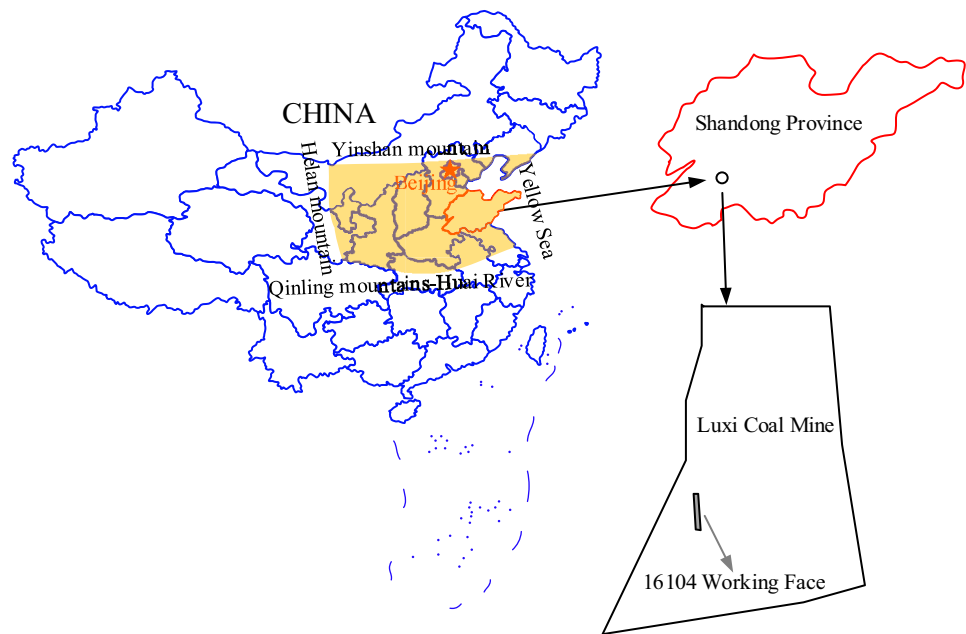
reinforced aquifers by grouting was deduced by Gao et al. (2020), and the 'three-stage casing' drilling with small angle was designed for fully grouting in the water-inrush danger zone determined by water-inrush coefficient (WIC) of working face floor, the 3D DC mine resistivity method was also used to check the effect of grouting. Using the fluid structure interaction (FSI) method in Flac^{3D}, Hu et al. (2019a, b, c, d) studied the pathway of water inrush around fault, under the coupled pressures of confined water and those induced by mining and the geophysical results indicated that the grouting was effective. Hu et al. (2019b) studied the slurry diffusion in the fractured aquifer grouted through horizontal injection holes, and established a theoretical model of slurry diffusion in the inclined tubular fractures, as well as the relationship between the distance of slurry diffusion and the grouting time. Li et al. (2017a) proposed a new water-inrush mechanism driven by grouting, and put forward an improved grouting solution based on statistical law of holes deviation for the prevention of water inrush from floor in coal mines with complicated geological conditions. These studies provide guidance to improve the grouting reinforcement the seam floor aquifers.

Since the concept of WIC and the evaluation index of water risk of the seam floor aquifers have been put forward, the study on grouting methods for controlling water inrush from the floor began in the 1950s (Li et al. 2018b). In Jiaozuo, Feicheng and other typical mining areas of China,

grouting in the underground tunnels was used to transform the floor aquifer and strengthen the crack structure.

However, the grouting effect of floor aquifer is not good because of the complex distribution of fracture networks (Ma et al. 2019, 2020a), unclear geological surveys, concealed grouting flow in rock mass fractures and improper engineering operations (Han et al. 2020). The secondary grouting not only causes the waste of materials, but also affects the construction period. Therefore, improving the overall efficiency of grouting and reducing the number of repeated times in the grouting process are the key technologies to ensure the safety of coal mining in the high-pressure aquifer.

Luxi coal mine is located in the southern area of Ningwen coalfield in Jining city, Shandong province, China. The #16 coal seam, which belongs to the Carboniferous system of the Taiyuan formation, is a planned coal seam. According to the standard of WIC, coal mining face will be threatened by aquifer water inrush during mining. Referring to relevant literature, water control measures of hydrophobic depressurization and grouting reinforcement have been widely proposed in previous studies. However, when aquifer has strong groundwater recharge source, hydrophobic depressurisation is difficult to achieve. Thus, the measures of hydrophobic depressurization are not suitable for OL aquifer under the coal mining with the large thickness, high-water pressure and water content, while the grouting reinforcement for floor aquifer can be used to guarantee of safe mining of #16 coal seam.

Geology and hydrology of the study area

Overview of the 16,104 working face

The Luxi coal mine is located in the southern Ningyang-Wenshang coal mining area, mainly located in Jining and Taian City, Shandong Province, China, a typical North China Coalfield, whose lower series coal is generally threatened by the thick OL aquifer. The Luxi coal mine is a modern mine with a production capacity of 870,000 metric tons per year. There are mainly three minable coal seams in the mine, including #3, #16 and #17 coal seam. The #3 coal seam will be replaced by #16 coal seam after the completion of mining. Now, the 16,104 working face, the first working face of #16 coal seam in the Ningyang-Wenshang coal mining area, has been formed. The 16,104 working face is about 900 m long along the strike and 100 m wide along the dip. The average thickness, average dip angle and buried depth of the 16,104 working face are 1.27 m, 1.35°, and 450 m, respectively. The intelligent mining-controlled system is used in 16,104 working face to ensure the safety and efficiency in the mining process.

Roof and floor structure of #16 coal seam

According to boreholes data of Luxi coal mine, there are three main limestone aquifers in the #16 coal seam roof and floor, i.e. the L_{10} limestone (L_{10}) aquifer, L_{14} limestone (L_{14}) aquifer of Carboniferous system Taiyuan formation and OL aquifer (Fig. 2). The other floor strata are mainly silty sandstone layers, fine sandstone layers and mudstone layers. The main roof, immediate roof, immediate and main floor are limestone, silty sandstone, mudstone and silty sandstone, respectively (Table 1).

The L_{10} aquifer

According to the previous geological data, the L_{10} aquifer is the direct water-filled aquifer, strong water abundance in individual regions. Its unit discharge is 0.0034–0.814 L/(s m) with an average of 0.382 L/(s m), and its permeability coefficient is 0.071–5.0899 m/d with an average of 1.09724 m/d. Underground water penetration accident will be happen by small probability, because the spray water is the main way of the L_{10} aquifer, which can be use as the necessary water for mining operation. Thus, the threat of water inrush of L_{10} aquifer to 16,104 working face can be relieved by release measures.

The L_{14} aquifer

The results showed that the L_{14} aquifer is an indirect water-filled aquifer through analyzed the formation structure of the roof and floor of 16,104 working face, which thick is
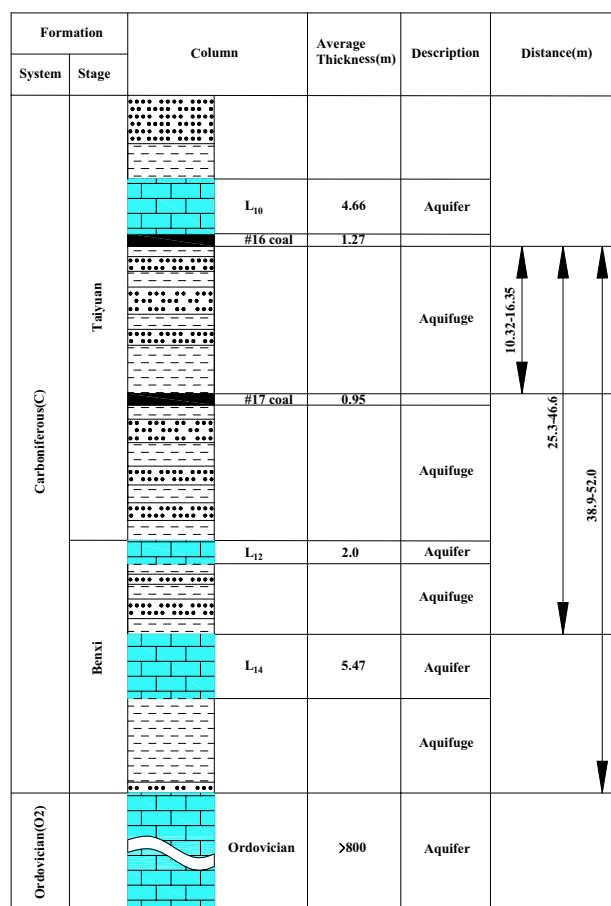

Fig. 2 Composite column of the 16,104 working face roof and floor

Table 1 Thickness of roof/floor

Roof/floor	Type	Thickness (m)	Average (m)
Main roof	Limestone	2.7–4.86	4.12
Immediate roof	Silty sandstone	2.3–6.22	4.66
Immediate floor	Mudstone	0.8–2.4	1.3
Main floor	Silty sandstone	1.0–2.5	1.5

2.3–10.7 m (5.47 m on average). It has weak water abundance according to the drill data, its unit discharge and permeability coefficient are 0.0002–0.03892 L/(s.m) and 0.003814–1.1275 m/d, respectively. However, according to the data in 2018 and 2019, the local water inflow of the aquifer is 100–200 m³/h, and the water pressure is 3.3–3.8 MPa. A certain hydraulic connection between L_{14} and OL aquifer based on the scouring experiment.

The OL aquifer

The OL confined aquifer is more than 800 m thick according to the data of the adjacent mine, with a maximum thickness

ranging up to 102.89 m in this hydrogeological area on the basis of exploratory data from drilling data, and karst fractures are more developed. Its unit discharge and permeability coefficient are 0.049–0.132 L/(s.m) and 0.094–0.1169 m/d, respectively, according to the pump test of surface boreholes. The relatively steady water level is + 15 to + 20 m (National Height Datum 1985), according to the scour experiment of underground boreholes. The OL aquifer, which has a range from low to high-water abundance according to 9 boreholes, is characterized by its uneven water abundance. Its water inflow is from 10 to 60 m³/h. The coal mining may be threatened greatly by the high-water pressure ranging from 4.1 to 4.2 MPa.

Physical and mechanical properties of floor rocks

Rocks of the lower part of Taiyuan and the upper part of Benxi formations in 16 coal seam floor is an ideal aquifuge, for the property of alternatively distributed soft and hard rock layers, stable sedimentary environment and weak water yield. On the whole, the interbedded structure of soft and hard rocks has high strength, it is more favorable for high impedance confined limestone water, considering the complex space structure of aquifuge. Then take into account the restraining factor of water inrush of the top of OL aquifer, which is undeveloped karst section, this interval can significantly improve the ability of coal seam floor to resist high-pressure water (Miao and Bai 2011).

Assessment of floor water inrush

The depth of floor failure

In the process of coal mining, the original rock stress state of surrounding rock is changed (Liu et al. 2020; Shi et al. 2019a, b; Ma et al. 2019, 2020b, 2021a). Cracks generation of the coal seam floor owing to water pressure of aquifer and support pressure, the increasing part of tangential stress owing to mining activity, may cause ground water bursting through the cracks (Li et al. 2019, 2017b; Ma et al. 2020a; Hu et al. 2019c). Therefore, it is of great significance to study the floor failure depth for prediction of the water inrush. At present, the floor failure depth is investigated with empirical formula, plastic mechanics and numerical simulation method (Liu et al. 2020). Next, the three methods were analyzed to calculate the failure depth of the floor.

Empirical formula method

For the floor failure depth of mining face, normally there are three common empirical formulas (State Bureau of Coal Industry 2000):

$$h_1 = 0.0085H + 0.1665\alpha + 0.1079L - 4.3579 \tag{1}$$

$$h_2 = 0.7007 + 0.1079L \tag{2}$$

$$h_3 = 0.303L^{0.8} \tag{3}$$

where h_1, h_2, h_3 are the floor failure depth, respectively, H is the buried depth of the coal seam, α is the angle of the coal seam, L is the length of the working face. Taking 450 m for H, 1.35° for α, 100 m for L, thus the floor failure depth is estimated as: $h_1 = 10.48$ m, $h_2 = 11.49$ m, $h_3 = 12.06$ m. To ensure safety, the maximum value of h_1, h_2 and h_3 is 12.06 m as the floor failure depth.

Plastic mechanics method

The area of floor failure caused by support pressure is shown in the Fig. 3, h_4 and L are the maximum floor failure depth and plastic zone width, respectively. According to the plasticity theory, the numeric symbols, 1, 2 and 3, stand for active stress zone, transition zone and passive stress zone, respectively.

The following calculation formula can be obtained (Qian et al. 2010):

$$h_4 = \frac{L}{2\cos\left(\frac{\pi}{4} + \frac{\phi}{2}\right)} e^{\left(\frac{\pi}{4} + \frac{\phi}{2}\right)\cdot\tan\phi} \cos\phi \tag{4}$$

where φ is the average internal friction angle of floor rock mass. According to the yield length of coal seam proposed by A. H. Wilson, the length of L can be calculated:
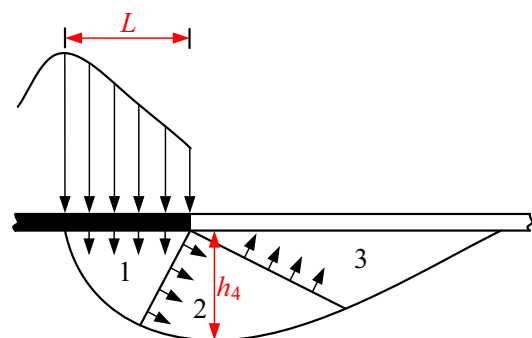
$$L = \frac{m}{F} \ln(10\gamma H) \tag{5}$$

Fig. 3 Area of floor failure zone due to support pressure

$$F = \frac{K-1}{\sqrt{K}} + \left(\frac{K-1}{\sqrt{K}}\right)^2 \cdot \tan^{-1}\sqrt{K} \tag{6}$$

Mohr–Coulomb criterion satisfied when coal seam reaches limit equilibrium conditions (Zhang and Zhang 1997),

$$K = \frac{1+\sin\phi_0}{1-\sin\phi_0} \tag{7}$$

By substituting Eqs. (6), (7) into (5), it was concluded that:

$$L = \frac{m\ln(10\gamma H)(1+\sin\phi_0)}{2\sin\phi_0\sqrt{\frac{1+\sin\phi_0}{1-\sin\phi_0}}\left(1 + \frac{2\sin\phi_0\sqrt{\frac{1+\sin\phi_0}{1-\sin\phi_0}}\tan^{-1}\sqrt{\frac{1+\sin\phi_0}{1-\sin\phi_0}}}{1-\sin\phi_0}\right)} \tag{8}$$

By substituting Eqs. (8) into (4), it was concluded that:

$$h_4 = \frac{m\ln(10\gamma H)(1+\sin\phi_0)e^{\left(\frac{\pi}{4}+\frac{\phi}{2}\right)\cdot\tan\phi}\cos\phi}{4\sin\phi_0\sqrt{\frac{1+\sin\phi_0}{1-\sin\phi_0}}\left(1 + \frac{2\sin\phi_0\sqrt{\frac{1+\sin\phi_0}{1-\sin\phi_0}}\tan^{-1}\sqrt{\frac{1+\sin\phi_0}{1-\sin\phi_0}}}{1-\sin\phi_0}\right)\cos\left(\frac{\pi}{4}+\frac{\phi}{2}\right)} \tag{9}$$

where m is the average mining height, γ is the rock mass density, φ_0 is the internal friction angle of coal. According to Fig. 2 and Table 2, taking φ as 40°, m as 1.27 m, γ as 24 kN/m³, φ_0 as 28°. The plastic zone width and the maximum floor failure depth can be obtained by Eqs. (8) and (9): $L = 12.92$ m, $h_4 = 12.82$ m.
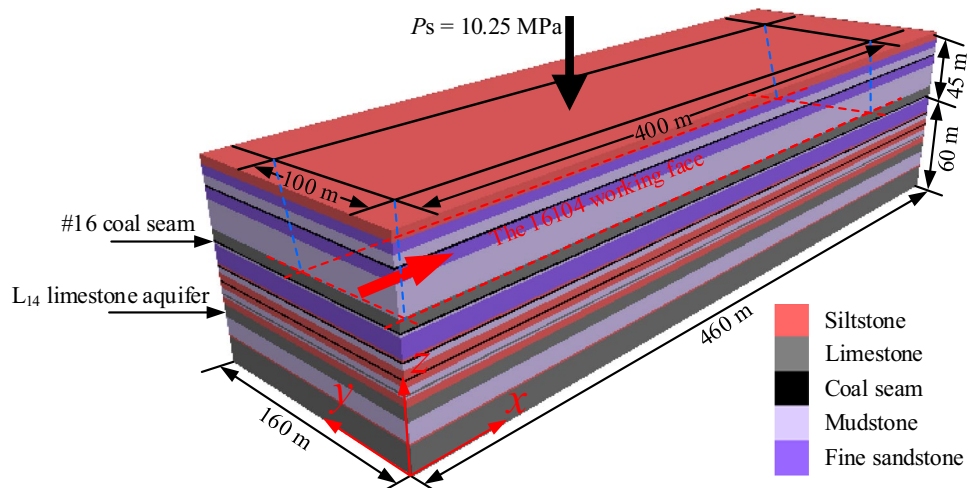
Numerical simulation

According to the geological and technical mining conditions in the region where the 16,104 working face is located, we constructed a FLAC³ᴰ numerical calculation model to study the influence of mining on floor failure depth of 16,104 working face (see Fig. 4). The stratification of the model is the same as the strata in Fig. 2. Physical and mechanical parameters of the rock used for modeling come from the measured parameters in the mining area, as shown in Tables 1 and 2. The calculation adopted the Moh-Coulomb criterion. Model dimensions were 460 m × 160 m × 110 m (length × height × high). The x- and y-axes represented the strike and dip directions, respectively; the z-axis was in the vertical direction. Cover depth was 45 m; extraction thickness (#16 coal seam) was 1.27 m. The thickness of the floor was 60 m.

Table 2 Rock mechanics index of the 16,104 working face floor

Lithology	Uniaxial compressive strength (MPa)	Tensile strength (MPa)	Bulk modulus (GPa)	Shear modulus (GPa)	Internal friction angle (°)	Cohesion (MPa)	Gravity (kg/m³)
Coal	25	0.31	6	5	28	2.03	2400
Mudstone	20	0.59	5	4	41	2.30	2450
Limestone	90	1.60	12	10	38	6.70	2660
Fine sandstone	50	2.28	7	6	39	5.91	2640
Siltstone	40	1.20	8	6	37	4.20	2540

Fig. 4 Numerical simulation model of 16,104 working face

Because this numerical simulation model was only about 110 m high, while the depth of cover was 455 m, an initial vertical principal stress (Ps) was applied to the top of model to simulate the weight of 410 m of overlying rock. Ps was calculated from

$$P_s = \gamma H \tag{10}$$

where γ is the bulk density of rock (average 25 kN/m^3 in China), and H is overburden thickness (m).

Equation (10) gives $P_s \approx 10.25$ MPa for these values. Since an elastic, isotropic model was assumed, the horizontal stress components were calculated by introducing Poisson's ratio. The base and lateral boundaries of the model were on rollers to simulate the initial stress field. Fixed base and lateral boundary conditions were used in subsequent excavation simulations.

The mining scheme modeled was as follows: longwall face 100 m in the y-direction; total face advance 400 m in the x-direction. The mining excavation space was located at the center of the model. Coal pillars 30 m wide were intentionally left to minimize boundary effects in both the x- and y-directions.

It can be seen from the Fig. 5a that the floor failure depth is 6 m when working face progressed at 20 m. Then, the floor failure depth increases with advance distance. The maximum floor failure depth of the 16,104 working face is 16 m when advanced distance is 40 to 100 m (Fig. 5b–d).

Based on the analysis of the above three calculation methods, the values obtained by empirical formula, plastic theory and numerical simulation method are 12.06 m, 12.82 m and 16.0 m, respectively (see Table 3). Therefore, taken 16.0 m as the value of floor failure depth in the 16,104 working face. According to the Fig. 2, the floor failure zone may extends to the #17 coal seam.

Possibility of water inrush based on the WIC

The probability of water inrush can be evaluated by the WIC when confined aquifer exists in the floor, according to mine water prevention relevant provisions, China (Li et al. 2018b; Ma et al. 2016, 2020a). The water-inrush risk existed of the floor if the WIC is more than the critical WIC (T_s). The formula of the WIC is as follows:

$$T = \frac{P}{M} \tag{11}$$

Table 3 Estimated results of the floor failure depth

Calculation	Empirical formula	Plasticity mechanics	Numerical simulation
Depth of failure zone (m)	12.06	12.82	16.0

(a) 20m
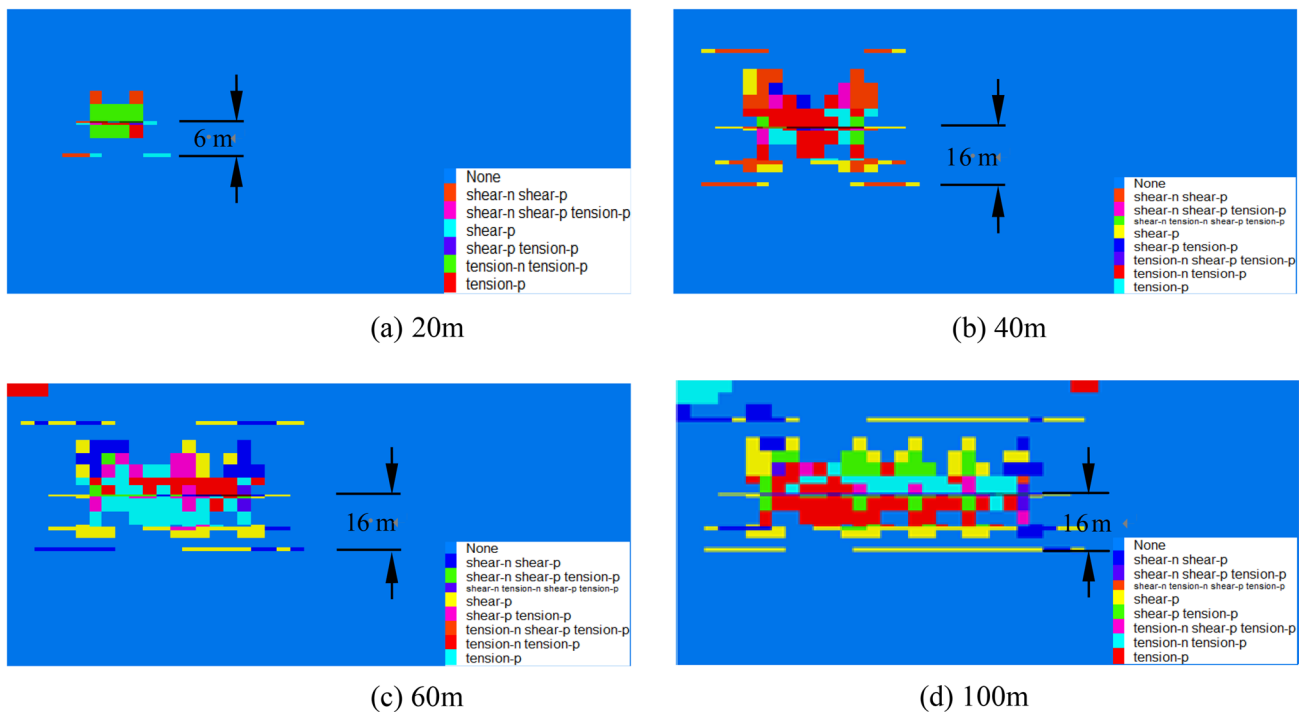

(b) 40m

(c) 60m

(d) 100m

Fig. 5 The floor failure depth with different advance distance of the 16,104 working face

Table 4 T values of the L_{14} and OL aquifer

Aquifer	P (MPa)	M (m)	H (m)	T (using Eq. 11) (MPa/m)	T (using Eq. 12) (MPa/m)
L_{14}	3.8	33	16	0.115	0.224
OL	4.2	46.5	16	0.09	0.138

where T is the WIC, P is the water pressure of the confined aquifer, M is the aquifuge thickness (State Bureau of Coal Industry 2000).

The research data of the national mine reveal that the T shall not be more than 0.06 MPa/m and 0.1 MPa/m where the floor is damaged by the structure or not in general, respectively.

Obviously, the above analysis has not considered the influence factors of mining. The effective thickness of aquiclude is reduced due to the floor failure depth under the influence of mining. The T considering the floor failure depth is as follows:

$$T = \frac{P}{M - h} \tag{12}$$

where h is the floor failure depth.

The floor is considered to be stable if the calculated result of the T is less than 0.1 MPa/m and 0.15 MPa/m in floor structural failure zone and without fracture structure, respectively. The T values of the L_{14} aquifer, OL aquifer are estimated using Eqs. (11) and (12).

It can be seen from the Table 4 that the T of L_{14} aquifer when Eqs. (11) or Eq. (12) is adopted are much higher than 0.1 and 0.15 MPa/m, respectively, which means that there is a high-water inrush possibility from the L_{14} aquifer. Although the T of OL aquifer is slightly less than 0.1

and 0.15 MPa/m, respectively, the average distance between the OL aquifer and the working face is 46.5 m (actual distance ranges from 38.9 to 52 m). The T of OL aquifer is also greater than the critical WIC if the minimum value is 38.9 m, thus the risk of water inrush also exists in the OL aquifer.

Geophysical and drilling results

According to the relevant provisions of coal mine water prevention in China, when the coal seam has the high-pressure karst aquifer and good water abundance in floor, geophysical and drilling exploration methods shall be used simultaneously. In this study, the Transient Electromagnetic Method (TEM) was used to detect the floor of the 16,104 working face within 0–150 m in December 2016. The results showed that there were two low-resistivity areas (areas a and b), as shown in Fig. 6. Area b was closer to #16 coal seam, which may have a greater impact on safety mining. The Radio Wave Penetration Method (RWPM) was employed to detect the floor in June 2017, and the water-rich areas (areas a, b, c, d and e) were obtained, as shown in Fig. 7. Then the Audio Frequency Perspective Method (AFPM) was used to determine the water-rich areas of water-bearing property of the floor, and four water-rich areas (areas a, b, c and d) were obtained. As presented in Fig. 8, area c was located in the middle of the 16,104 working face, and area d was close to the open-off cut.

Based on the results of the three geophysical prospectings, it was found that water-rich areas existed in the floor of the middle of the 16,104 working face and open-off cut position. To reduce the risk of water inrush caused by the water-rich areas during the mining process, the gateway of the 16,104 working face was redesigned, which was

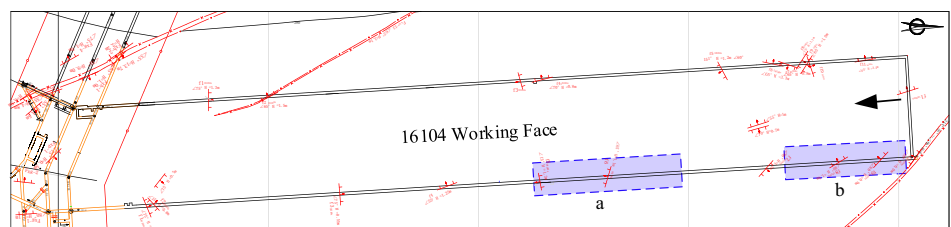**Fig. 6** The water-rich areas of the 16,104 working face in floor detected by TEM

Fig. 7 The water-rich areas of the 16,104 working face in floor detected by RWPM
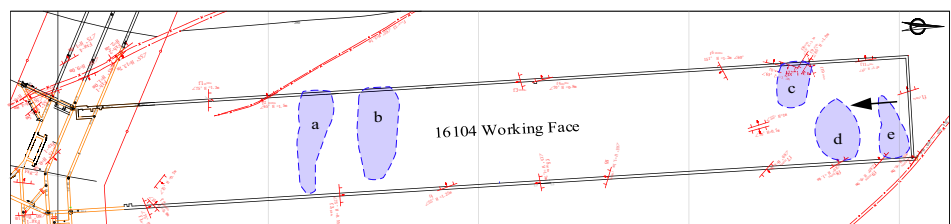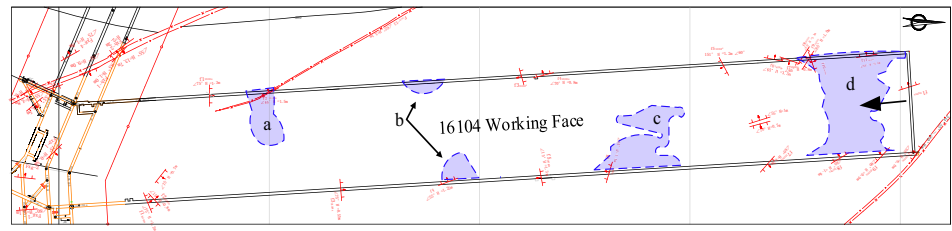
Fig. 8 The water-rich areas of the 16,104 working face in floor detected by AFPM

shortened from 140 to 100 m in dip and 1400–900 m in strike (see Fig. 11). As a result, some water-rich areas of limestone aquifer were avoided, the floor failure depth of was reduced, and the risk of water inrush from the floor aquifer was reduced.

To verify the water-rich areas obtained by the geophysical prospecting method, 56 boreholes were drilled in the L_{14} aquifer in Year 2018 and the water inflow was analyzed (see Table 5). Figure 9 shows the 55 grouting holes arrangement of the 16,104 working face in 2018. As shown in Fig. 10,

these boreholes were grouped by the water inflow, and the amount of water inflow above 10 m³/h and exceed 100 m³/h were 94.64% and 50%, respectively.

Figure 11 shows the contour map of water inflow based on the 56 boreholes of L_{14} aquifer. It can be seen that two areas (areas *a* and *b*) with a large amount of water inflow are located in the middle of the upper gateway and the intersection of the lower gateway and the open-off cut, respectively. However, areas *a* is not shown in Fig. 8. The reasons are as follows: (a) The occurrence state of

Table 5 Detection data of test holes (in year 2018)

Hole no	Vertical depth (m)	Water inflow (m³/h)	Water pressure (MPa)	Hole no	Vertical depth (m)	Water inflow (m³/h)	Water pressure (MPa)
1#	31.4	13	3.2	29#	30.7	25	3.7
2#	35.2	4	3.45	30#	28.2	65	3.3
3#	39.3	5	3.2	31#	27.6	100	3.2
4#	29.7	15	3.45	32#	24.1	150	3.25
5#	25.2	13	3.4	33#	33.1	120	3.3
6#	34.4	120	3.4	34#	27.6	80	3.3
7#	35.9	110	3.4	35#	35.5	20	3.8
8#	34.1	100	3.4	36#	35.8	120	3.65
9#	27.8	80	3.2	37#	30.7	150	3.68
10#	36.6	50	3.25	38#	35.4	130	3.7
11#	27.8	100	3.4	39#	39.2	20	3.6
12#	31.9	100	3.4	40#	33	70	3.65
13#	32.3	100	3.3	41#	27.8	130	3.7
14#	28.1	2	3.3	42#	29.1	100	3.7
15#	26.5	50	3.4	43#	32.1	65	3.65
16#	27.8	200	3.25	44#	30.4	80	3.7
17#	34.5	20	3.3	45#	33.6	60	3.7
18#	36.5	120	3.2	46#	30.9	100	3.7
19#	30.6	150	3.3	47#	31.5	80	3.75
20#	36.8	120	3.25	48#	30	20	3.75
21#	28.9	40	3.2	49#	29.8	100	3.7
22#	26.5	120	3.25	50#	28.6	95	3.6
23#	36.1	100	3.25	51#	24.5	20	3.7
24#	45.1	200	3.2	52#	32.1	200	3.7
25#	32.2	80	3.25	53#	33.6	150	3.6
26#	32.2	40	3.2	54#	29.5	150	3.6
27#	39.4	30	3.25	55#	23.8	150	3.8
28#	25.4	120	3.25	56#	29.7	10	3.5

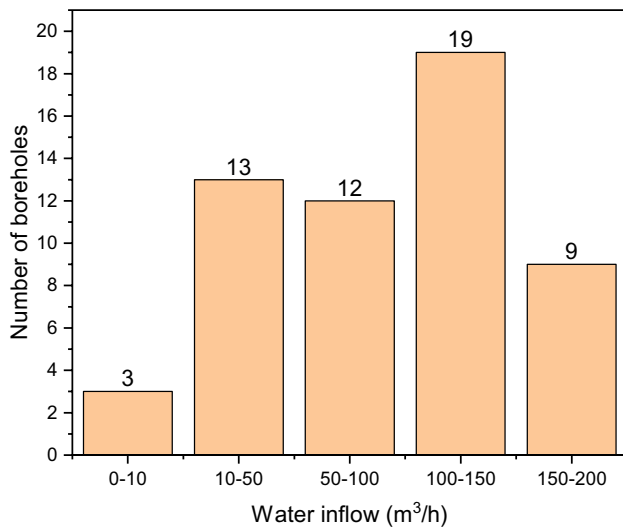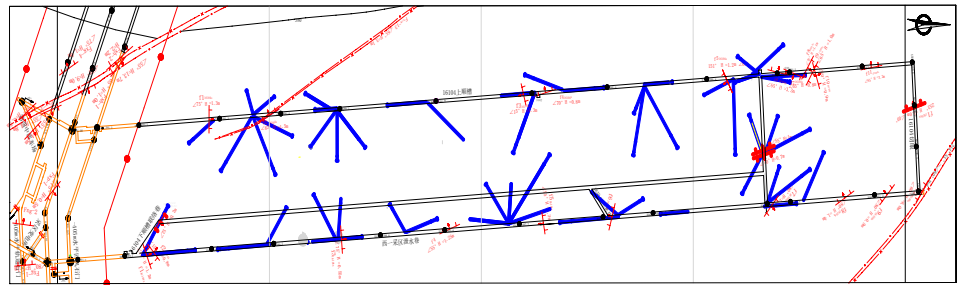**Fig. 9** Layout of 55 grouting holes of the 16,104 working face in Year 2018

Fig. 10 Number of boreholes with different water inflow

groundwater changes with time. The geophysical exploration was completed in Years 2016 and 2017, while the drilling was in Year 2018. (b) The drilling can also affect the occurrence state of groundwater. The original non-water-conducting fractures were gradually connected by boreholes, and the water content in the areas increased significantly.

The risk of water-inrush risk in the 16,104 working face is analyzed using Eqs. (11) and (12). As shown in Fig. 12a–b, the T of all boreholes exceed 0.06 MPa/m, and 64.29% of them are greater than 0.1 MPa/m. If the floor failure depth was considered, the T of all boreholes
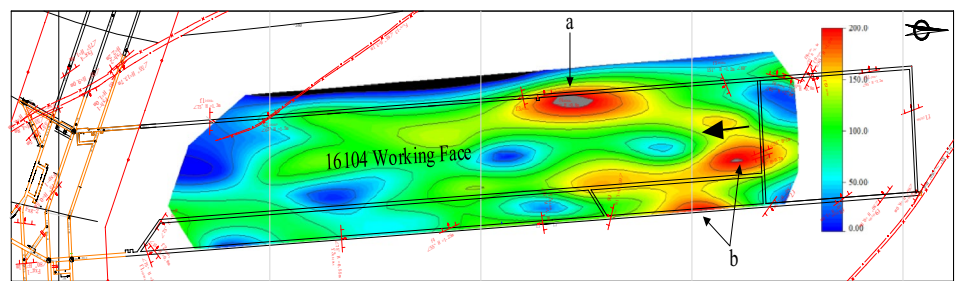
exceed 0.06 MPa/m, and the proportion of that exceeding 0.15 MPa/m is even higher at 96.43%.

In 2018, 55 boreholes were grouted and reinforced in the 16,104 working face, and only 1 borehole was reserved as observation hole to observe water pressure of the L_{14} aquifer. A total of 745 tons of cement were injected, with an average of 13.55 tons per borehole. The grouting effect was detected by the Network Parallel Electrical Method (NPEM) in May 2019. Through the NPEM method, four water-rich areas were found in the range of 0 to 45 m from the floor of the working face. The water-rich areas were projected on the plan of the 16,104 working face, that is, areas a, b, c and d in Fig. 13a. The wider area a is distributed in the lower gateway with a range of 630–860 m (starting from the open-off cut), and an extension of about 50–90 m along with the profile. Since the apparent conductivity was obviously higher than the critical threshold (10.4S/m) in area a, it was verified that rock fractures were well-developed and the groundwater was abundant in area a. Area b was located at 400–550 m in the upper gateway and 380–460 m in the lower gateway, extending to about 50 m and 40 m of the 16,104 working face, respectively. Area b was characterized by the smaller range and low electrical resistivity, and it was believed that the L_{14} aquifer was rich in water. As shown in Fig. 13b, the other two areas have low electrical resistivity, i.e., area c (300–330 m in the upper gateway) and area d (0–100 m in the upper gateway and 50–137 m in the open-off cut). According to water inflow data in 2018, it is determined that there were micro-fractures in areas a and b.

The results revealed that there were also four areas of low electrical resistivity in the range of 45—90 m under the floor, i.e., areas a, b, c and d in Fig. 13b. Among them, area

Fig. 11 Contour map of water inflow in L_{14} aquifer
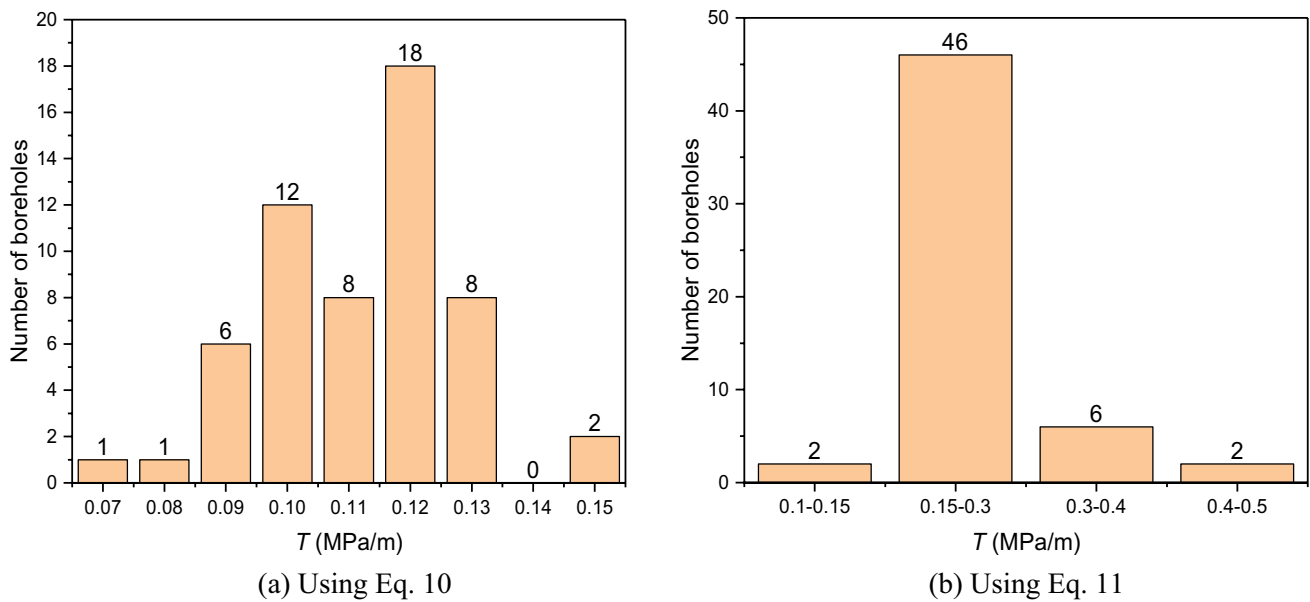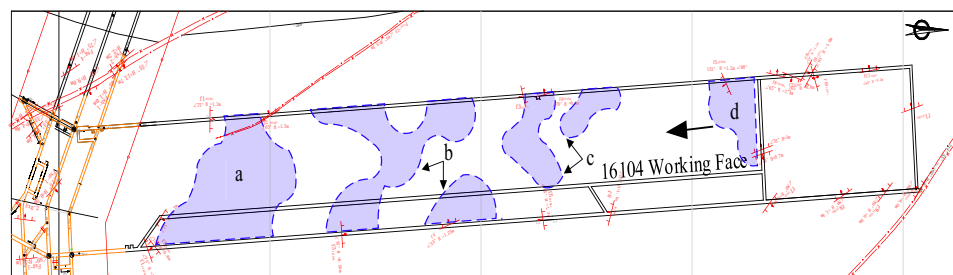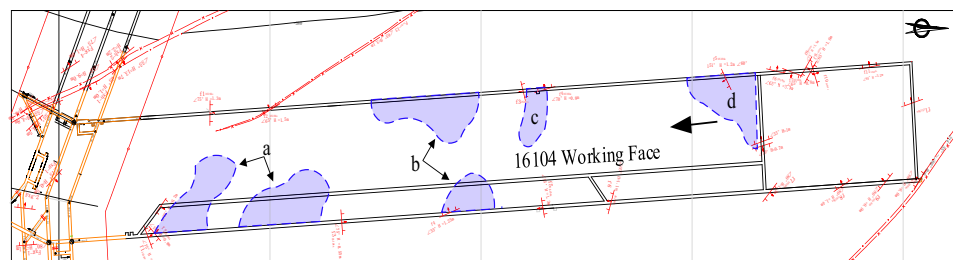
(a) Using Eq. 10

(b) Using Eq. 11

Fig. 12 Number of boreholes with different WIC of the L_{14} aquifer

Fig. 13 The water-rich areas of 16,104 working face in floor detected by NPEM

(a) in the range of 0-45 m

(b) in the range of 45-90 m

a was located in the upper gateway (710–760 m) and the lower gateway (690–860 m), running through the working face along the inclined direction. Area *a* in Fig. 13b had a significantly larger distribution range than area *a* in Fig. 13a. Areas *b* and *c* in Fig. 13b were roughly divided into two areas. Compared with the two areas in Fig. 13a, the range of areas *b* and *c* were obviously expanded, and the water-rich areas increased. It indicated that the water abundance within

the range of 45–90 m was enhanced. The spatial distribution of area *d* was similar to that in Fig. 13a, while the shape of area *d* was slightly changed.

Based on water-rich areas delineated by the NPEM, 39 drilling holes were designed for grouting reinforcement of the L_{14} aquifer in Year 2019. Table 6 shows the water inflow and pressure of 39 drilling holes. Figure 14 shows

the arrangement of 39 grouting holes in the 16,104 working face in Year 2019.

Figure 15 shows the contour map of water inflow based on the data of 39 boreholes (the contour map is not fully show the whole working face due to the limited number of boreholes). The water-rich areas *a* and *b* in Fig. 11 have disappeared, but a new area was generated in the middle of the gateway.

Compared with the water inflow in Fig. 10, the proportion of water inflow above 10m^3/h and 100m^3/h decreased in

Fig. 16. After grouting, water inflow and WIC of the 16,104 working face are analyzed by Eqs. (11) and Eq. (12), as shown in Fig. 17a–b. The WIC of all the boreholes is greater than 0.06 MPa/m through the calculation of Eqs. (11) and Eq. (12). According to Eq. (10), the WIC of 21 boreholes is over 0.1 MPa/m, accounting for 53.8% of the total. According to Eq. (12), the WIC of 36 boreholes is greater than 0.15 MPa/m, accounting for 92.3%. The results showed that 55 boreholes have little effect on water inflow compared to the water flow before grouting for the floor reconstruction.

Table 6 Detection data of test holes (in 2019)

Hole no	Vertical depth (m)	Water inflow (m^3/h)	Water pressure (MPa)	Hole no	Water inflow (m^3/h)	Water pressure (MPa)
4–1	30.3	60	3.4	7–7	20	3.5
4–2	26.9	80	3.5	7–8	120	3.5
4–3	39.4	150	3.7	8–1	3	3.5
4–4	45.1	0.3	3.3	8–2	10	3.5
4–5	28.1	80	3.6	8–3	180	3.5
5–1	28.7	30	3.5	8–4	60	3.6
5–2	34	120	3.5	9–1	20	3.55
5–6	42	20	3.7	9–2	20	3.5
6–1	32.9	2	3.3	9–4	50	3.6
6–2	35.5	5	3.5	10–1	40	3.7
6–4	36.8	2	3.8	10–2	0.5	3.7
6–5	32.9	7	3.3	10–3	90	3.7
6–6	34.9	10	3.5	10–4	60	3.5
6–7	35.4	20	3.5	10–5	50	3.3
6–8	34.4	180	3.3	10–6	200	3.6
7–1	32.7	190	3.6	10–7	2	3.5
7–3	42.4	60	3.5	11–1	50	3.5
7–4	25.4	80	3.6	11–2	50	3.5
7–5	29	40	3.5	11–3	3	3.5
7–6	28.1	10	3.5			

Fig. 14 Layout of 39 grouting holes of the 16,104 working face in Year 2019

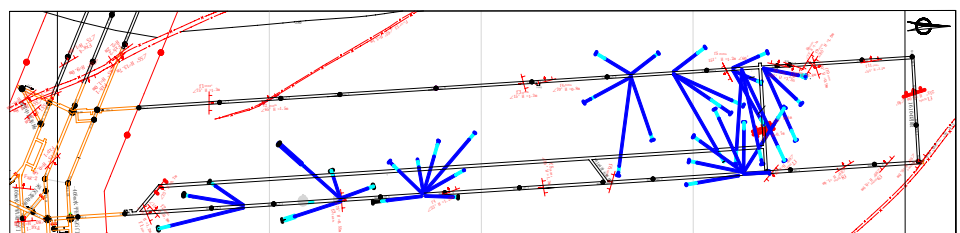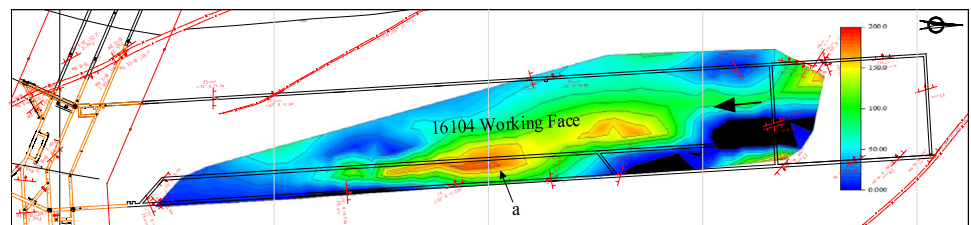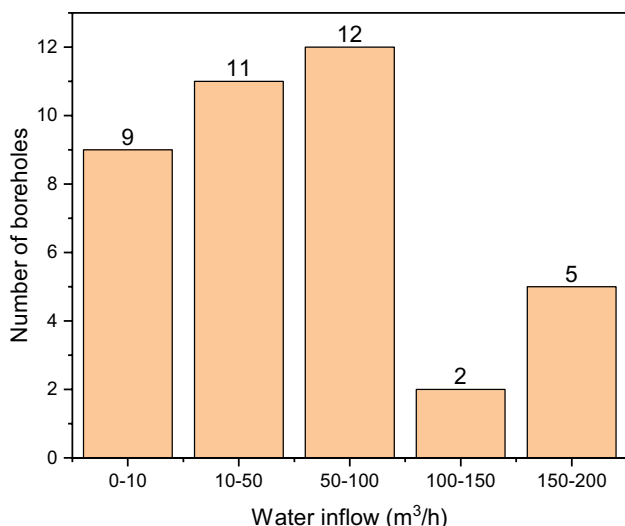**Fig. 15** Number of boreholes with different water inflow

Fig. 16 Number of boreholes with a different water inflow

Grouting reinforcement techniques of floor aquifer

Grouting diffusion in rock fractures

It can be seen from the above analysis that water inflow restrained by grouting is not effective, and the main reasons are as follows: rock fractures in the coal measures aquifer are not isolated, and a group of rock fractures is usually formed according to a certain occurrence; in the grouting process, adjacent fractures interfere with each other, and the control effect of grouting is weakened. The larger fracture is further opened compared with a single fracture, and the influence of interaction between parallel fractures has a great influence on the smaller fracture. With the increase of grouting time, the small fracture tends to be closed under the high pressure and squeezing action of the larger fracture (see Fig. 19).

For the large fractures in the actual project, a longer diffusion distance of the grouting is caused due to the further increase of the fracture width. While spreading distance in the small fracture is limited or cannot be injected owing to narrowing fracture width, then small fractures are unable to be sealed. After the grouting pressure decreases, the larger cracks are closed again under the action of ground stress, and the closure degree of fractures depends on the property of the grouting.

If the grout has been solidified after grouting, the consolidating body will occupy part of the fracture, and effectively block the water passageway (Zheng et al. 2015). If the grout has good fluidity, it may migrate deeply in space under the compression of rock masses; then the closed smaller fracture

As shown in Fig. 18, the proportion of boreholes with water inflow greater than 100 m^3/h decreases significantly, but the proportion of boreholes with water inflow between 10 and 50 m^3/h increases. The T (using Eq. 11) of 21 boreholes and the T (using Eq. 12) of 36 boreholes are greater than 0.1 and 0.15 MPa/m, respectively. Thus, the grouting effect has not met the requirements.
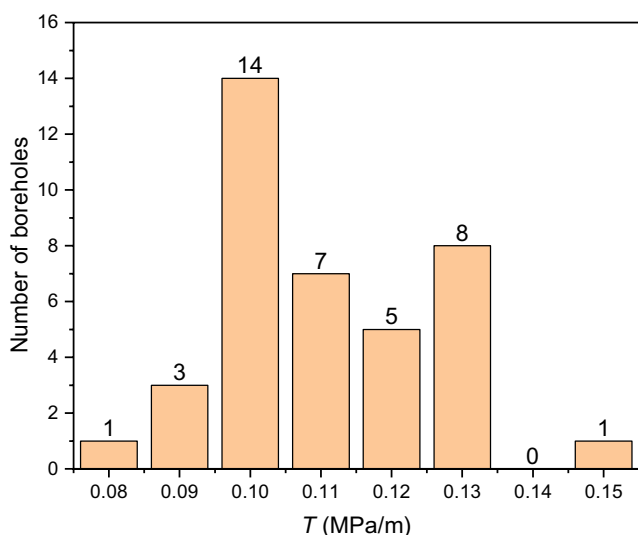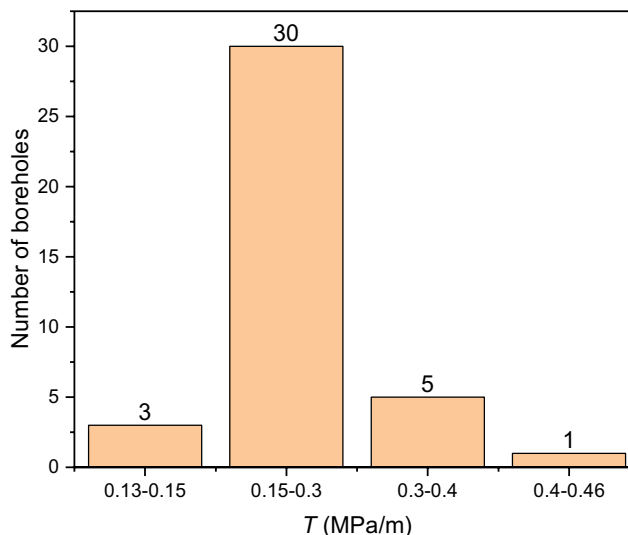

(a) Using Eq. 1

(b) Using Eq. 2

Fig. 17 Number of boreholes with different water-bursting coefficient (T) of the L$_{14}$ limestone
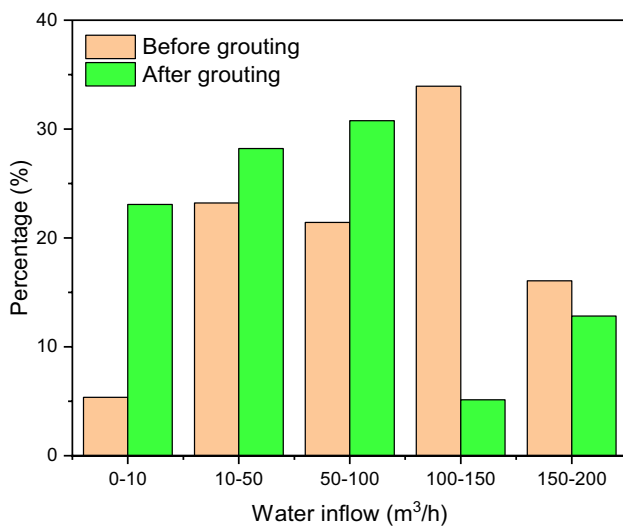
Fig. 18 Comparison of the percentage of the water inflow of the L_{14} of the 16,104 working face in floor before and after grouting

under the compression of larger fracture will be reopened, forming the water flow channel. Thus, sealing efficiency cannot be improved only increase grouting pressure. To completely seal the water flow channels, secondary or supplementary grouting is needed (Fig. 20).

Secondary grouting-reinforcement method

To enhance overall grouting efficiency and reduce the repeat numbers of grouting in the floor aquifer, a secondary grouting-reinforcement method is proposed to ensure the effective injection of massive grout into the aquifer. The goal of secondary reinforcement is realized by the method of secondary grouting reinforcement. The method can be performed as follows: (1) borehole scouring and flushing; (2) the injection of slurry, concentrate, slurry and water; (3) fresh water perfusion; (4) borehole sealing and sweeping. First, after the drilling reaches the design length, the borehole can be plugged by grouting if the water inflow is less than 5 m^3/h; otherwise, the borehole shall be continuously drained until the water inflow is stable. It is noteworthy that the boreholes should be flushed with clear water to ensure that rock powder and rock block are washed out of the boreholes. The following step is extremely important in the secondary grouting-reinforcement method. The slurry is adjusted to a concentration of 1.1–1.3 g/cm^3 and the injection pressure is adjusted to above 7.0 MPa; the concentration of the slurry is increased to 1.3–1.5 g/cm^3 and pressure reaches 8.0 MPa; after that, the concentration is reduced to 1.1–1.3 g/cm^3 and pressure increases to 9.0 MPa. Fresh water test is carried out, the pressure reaches 9.0 MPa after the grouting pressure and then keeps stable. The concentrate is used to seal the borehole and setting time should no less than 24 h. Finally, the borehole grouted is examined, that is, borehole sweeping, which can play a positive effect on the test of grouting effect. The expected grouting effect can be achieved if the water inflow of the tested borehole is less than 5 m^3/h, with enough plugging; otherwise, the borehole needs to be flushed and grouted again (the grouting method is the same as the first grouting). It is worth noting that the secondary grouting, i.e., borehole flushing and grout injection, is carried out after the first grouting process is completed. It means that the secondary drilling and secondary grouting are required at the location of the first grouting.

Table 7 shows that the results of seven grouting boreholes by secondary grouting-reinforcement method. As mentioned above, the sealing quality was considered safe if water flow of a single test hole was lower than 5m^3/h. The results of the water inrush from the boreholes reinforced by the secondary grouting-reinforcement method show that this method is effective for controlling water.
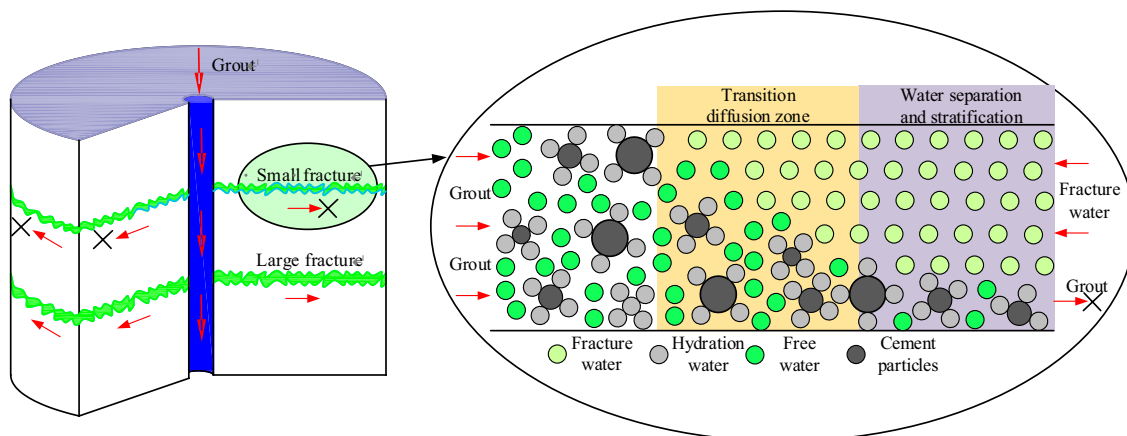

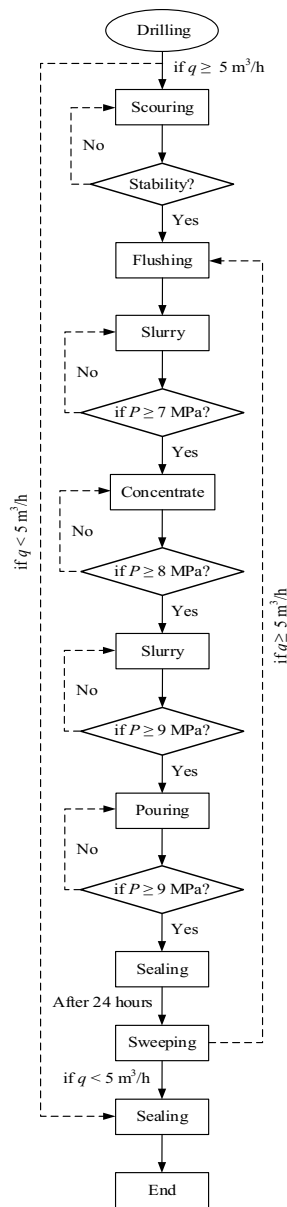**Fig. 19** Flow model of grout in fractures (Zhang 2011)

Fig. 20 Grouting process

Discussions

Grouting has been widely applied to the floor in a coal mine for the prevention and control of water inrush (Hu et al. 2020; Liu et al. 2020). Due to the imperfection of grouting technologies, some grouting boreholes fail to achieve the expected effect after the full-floor grouting project in a coal mine. As a result, these failed grouting boreholes have become a hidden danger in mining.

For example, in the Yian coal mine (a new mine in Luoyang city, Henan province, China), the fully sealed sealing method has been used for the borehole sealing method of floor grouting reinforcement, that is one-time grouting completion method, and the defect rate was as high as 53–57%. The grouting effect has not been achieved because of a large amount of water outflow from the boreholes.

The risk of water inrush caused by grouting boreholes in mining mainly depends on whether the boreholes have been blocked effectively or not. The boreholes will have higher hydraulic conductivity if the grouting effect is poor or the diffusion distance is shorter. When such boreholes are approached or exposed by mining, the water flow channel of 'Confined aquifer-Conducted water borehole-Primary or secondary fractures-Working face' will be formed under the connection of primary or secondary fractures (see Fig. 21a). The working face will be affected if the water in the confined aquifer discharges into the working face along the boreholes. In the process of water inrush, the water diversion channel is constituted by the basic elements, confined aquifer, conducted water boreholes, primary or secondary fractures and the working face.

Most of the engineers believe that grouting is an effective way to control coal mine water in China. However, they are not aware that the unreasonable grouting technology will increase water inflow, and may cause serious water inrush due to the connectivity of grouting boreholes (Kang et al. 2014; Wang et al. 2015). In the engineering practice, grouting materials and the diffusion radius are

Table 7 The results by secondary grouting-reinforcement method

Hole no	First drilling			Sweeping (secondary drilling)			Sweeping (thirdly drilling)	Meet the requirements (<5 m³/h)
	Water inflow (m³/h)	Water pressure (MPa)	Grouting quantity (Ton)	Water inflow (m³/h)	Water pressure (MPa)	Grouting quantity (Ton)	Water inflow (m³/h)	
X4-4z	60	3	10.1	45	3	57	2	Yes
X4-6z	60	3.7	10.25	40	3.7	127	0.6	Yes
X5-1Z	165	3.5	12.75	70	3.5	67	1	Yes
X5-5Z	100	3.5	12.6	40	3.5	17.3	1	Yes
X5-6Z	110	3.5	12.75	50	3.5	40.45	2	Yes
X7-1Z	191	3.4	18.6	40	3.4	46.5	0.5	Yes
X7-2Z	97	3.4	5.9	30	3.4	19.6	0.02	Yes

Fig. 21 Comparison of grouting effect between the suffocating method and the secondary grouting method
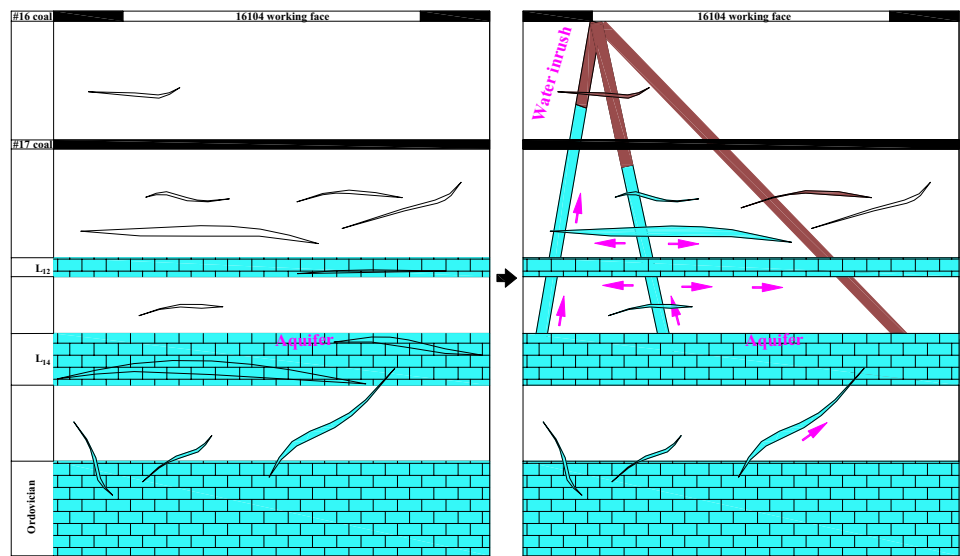
(a) Floor water flow channels caused by failed grouting process
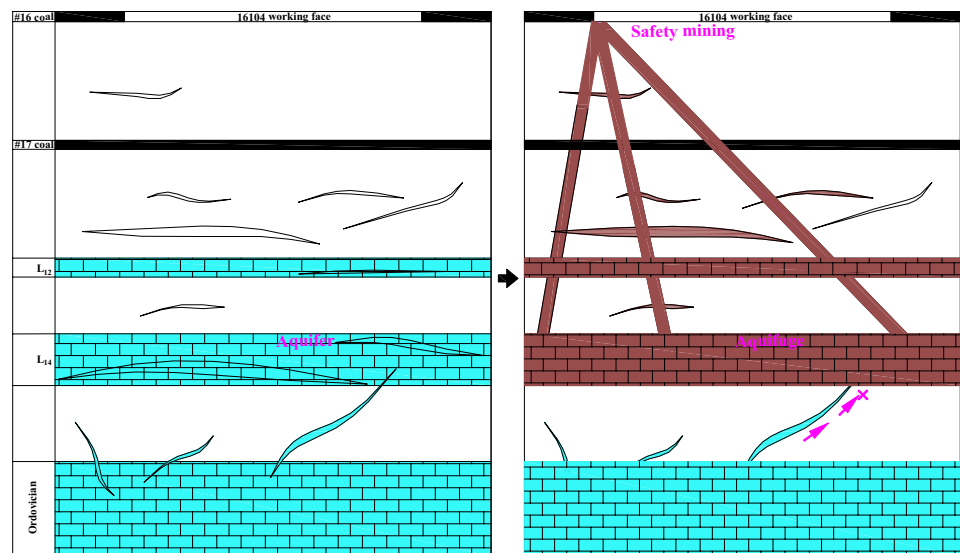
(b) L$_{14}$ is transformed into aquifuge by secondary grouting method

mainly concentrated, which can partially prevent the floor water inrush under the low water pressure aquifer (Li et al. 2017a). The opened fractures to the main seepage path should be filled firstly, and the unopened fractures can be are neglected or partly filled after solidification under grout pressure. Nevertheless, when grouting is performed in an aquifer with high-water pressure, grout with a high concentration will lose water due to the high grouting pressure, and the cement particles will be consolidated quickly, thus impeding the flow of grout. As a result, the gradual increase of grouting pressure gives an illusion that the effect has been achieved (such as the 16,104 working face, Luxi coal mine in this paper). In this study, the number of regrouting boreholes

and cost can be reduced by the investigation and analysis of secondary grouting technology. Besides, the quality and speed of grouting at the working face can be ensured by the secondary grouting technology, and the grouting practice in this study offers a reference for grouting engineering (see Fig. 21b).

Conclusions

(1) In the 16,104 working face, the water-rich areas of seam floor aquifer obtained by geophysical methods and the areas with large water inflow by drilling holes have dif-

ferences. When water-rich areas obtained by geophysical methods are taken as the key grouting areas, the grouting effect is not satisfactory. As an indirect prospecting method, the geophysical method is affected by many factors. Therefore, the results of geophysical and drilling methods should be simultaneously evaluated when the grouting reconstruction technique is applied to the floor aquifer.

(2) Excessive grouting boreholes may have a serious impact on the position of water-rich areas of seam floor aquifer. Grouting boreholes can connect the water-conducting fractures of several disjoint areas. Then the water content of connected fractures increases, that is, water-bearing capacity of the weak aquifer is enhanced. The water-inrush accidents are more likely to occurs if the expected effect is not achieved.

(3) A secondary grouting method for floor aquifer of coal seams is proposed to ensure the injection amount of grout into the confined aquifer. In the proposed method, the grouting flow is increased, verification holes are reduced, the goal of preventing water inrush from floor aquifer in mining progress can be realized.

(4) A reinforcement method of floor grouting in the high-water pressure working face of coal mines is proposed to ensure amount of grout injected into the confined aquifer. The method plays a role in check the grouting effect, increase the grouting flow and reduce verification holes, thus to achieve the goal of preventing water inrush from floor aquifer in mining progress.

References

Cao SG, Li GF, Yao QL, Wang FH (2009) Prediction of quantity of water inrush from coal seam floor and its reinforcement technique by grouting. Chin J Rock Mech Eng 28(2):312–318. https://doi.org/10.13722/j.cnki.jrme.2009.0312

Dong SN, Wang H, Zhang WZ (2019) Judgement criteria with utilization and grouting reconstruction of top Ordovician limestone and floor damage depth in North China coal field. J China Coal Soc 44(7):2216–2226. https://doi.org/10.13225/j.cnki.jccs.2018.1107

Dong SN, Zheng LW, Tang SL, Shi PZ (2020) A scient metric analysis of trends in coal mine water inrush prevention and control for the period 2000–2019. Mine Water Environ 39:3–12. https://doi.org/10.1007/s10230-020-00661-2

Gao WF, Shi LQ, Han J, Zhai PH (2020) Study on control water of Ordovician aquifer: a coal mine of Feicheng mining area. China Carbonate Evaporite 35:48. https://doi.org/10.1007/s13146-020-00588-3

Guo BH, Cheng T, Wang L, Luo T, Yang XY (2018) Physical simulation of water inrush through the mine floor from a confined aquifer. Mine Water Environ 37:577–585. https://doi.org/10.1007/s10230-017-0488-7

Han CH, Zhang WJ, Zhou WW, Guo JB, Fi Y, Man XQ, Jiang JG, Zhang CR, Li YJ, Wang Z, Wang H (2020) Experimental investigation of the fracture grouting efficiency with consideration of the viscosity variation under dynamic pressure conditions. Carbonate Evaporite 35:30. https://doi.org/10.1007/s13146-020-00568-7

Hu YB, Li WP, Wang QQ, Liu SL, Wang ZK (2019a) Study on failure depth of coal seam floor in deep mining. Environ Earth Sci 78:697. https://doi.org/10.1007/s12665-019-8731-0

Hu YB, Li WP, Wang QQ, Liu SL, Wang ZK (2019b) Evaluation of water inrush risk from coal seam floors with an AHP–EWM algorithm and GIS. Environ Earth Sci 78:290. https://doi.org/10.1007/s12665-019-8301-5

Hu YB, Li WP, Wang QQ, Liu SL, Wang ZK (2019c) Evolution of floor water inrush from a structural fractured zone with confined water. Mine Water Environ 38:252–260. https://doi.org/10.1007/s10230-019-00599-0

Hu Y, Jian S, Liu WQ, Wei DY (2019d) The evolution and prevention of water inrush due to fault activation at working face No. II 632 in the Heng yuan coal mine. Mine Water Environ 38:93–103. https://doi.org/10.1007/s10230-018-00579-w

Hu Y, Liu WQ, Shen Z, Gao K, Liang DX, Cheng SX (2020) Diffusion mechanism and sensitivity analysis of slurry while grouting in fractured aquifer with horizontal injection hole. Carbonate Evaporite 35:49. https://doi.org/10.1007/s13146-020-00587-4

Kang YS, Liu QS, Gong GQ, Wang HC (2014) Application of a combined support system to the weak floor reinforcement in deep underground coal mine. Int J Rock Mech Min Sci 71:143–150. https://doi.org/10.1016/j.ijrmms.2014.03.017

Li H, Bai HB, Wu JJ, Wang CS, Ma ZG, Du YB, Ma K (2017a) Mechanism of water inrush driven by grouting and control measures-a case study of Chensilou mine. China Min Water Environ 10:468. https://doi.org/10.1007/s12517-017-3258-8

Li H, Bai HB, Wu JJ, Zhao HM, Ma K (2017b) A method for prevent water inrush from karst collapse column: a case study from Sima mine. China Environ Earth Sci 76:493. https://doi.org/10.1007/s12665-017-6831-2

Li T, Gao Y, Chen W (2018a) Characteristics of deep Ordovician limestone water and its concentrated application in Ordovician limestone water disaster prevention. J China Coal Soc 43(S1):262–268. https://doi.org/10.13225/j.cnki.jccs.2017.3001

Li WP, Liu Y, Qiao W, Zhao CX, Yang DD, Guo QC (2018b) An improved vulnerability assessment model for floor water bursting from a confined aquifer based on the water inrush coefficient method. Mine Water Environ 37:196–204. https://doi.org/10.1007/s10230-017-0463-3

Li H, Bai HB, Wu JJ, Meng QB, Ma K, Wu LY, Meng FF, Wang SJ (2019) A set of methods to predict water inrush from an Ordovician karst aquifer: a case study from the Chengzhuang mine, China. Mine Water Environ 38:39–48. https://doi.org/10.1007/s10230-018-00572-3

Liu SQ, Fei Y, Xu YC, Huang L, Guo WY (2020) Full-floor grouting reinforcement for working faces with large mining heights and high-water pressure: a case study in China. Mine Water Environ 39(2):268–279. https://doi.org/10.1007/s10230-020-00683-w

Ma D, Bai HB (2015) Groundwater inflow prediction model of karst collapse pillar: a case study for mining-induced groundwater inrush risk. Nat Hazard 76:1319–1334. https://doi.org/10.1007/s11069-014-1551-3

Ma D, Miao XX, Bai HB, Pu H, Chen ZQ, Liu JF, Huang YH, Zhang GM, Zhang Q (2016) Impact of particle transfer on flow properties of crushed mudstones. Environ Earth Sci 75:593. https://doi.org/10.1007/s12665-016-5382-2

Ma D, Wang JJ, Cai X, Ma XT, Zhang JX, Zhou ZL, Tao M (2019) Effects of height/diameter ratio on failure and damage properties of granite under coupled bending and splitting deformation. Eng Fract Mech 220:106640. https://doi.org/10.1016/j.engfracmech.2019.106640

Ma D, Duan HY, Liu WT, Ma XT, Tao M (2020a) Water-sediment two-phase flow inrush hazard in rock fractures of overburden strata during coal mining. Mine Water Environ 39:308–319. https://doi.org/10.1007/s10230-020-00687-6

Ma D, Duan HY, Zhang Q, Zhang JX, Li WX, Zhou ZL, Liu WT (2020b) A numerical gas fracturing model of coupled thermal, flowing and mechanical effects. Comput Mater Contin 65(3):2123–2141. https://doi.org/10.32604/cmc.2020.011430

Ma D, Kong SB, Li ZH, Zhang Q, Wang ZH, Zhou ZL (2021a) Effect of wetting-drying cycle on hydraulic and mechanical properties of cemented paste backfill of the recycled solid wastes. Chemosphere 282:131163. https://doi.org/10.1016/j.chemosphere.2021.131163

Ma D, Zhang JX, Duan HY, Huang YL, Li M, Sun Q, Zhou N (2021b) Reutilization of gangue wastes in underground backfilling mining: overburden aquifer protection. Chemosphere 264:128400. https://doi.org/10.1016/j.chemosphere.2020.128400

Miao XX, Bai HB (2011) Water-resisting characteristics and distribution rule of carbonate strata in the top of Ordovician in North China. J China Coal Soc 36(2):185–193. https://doi.org/10.13225/j.cnki.jccs.2011.02.004

Qian MG, Shi PW, Xu JL (2010) Ground pressure and strata control. China University and Technology Press, Xuzhou

Qian MG, Xu JL, Wang JC (2018) Further on the sustainable mining of coal. J China Coal Soc 43(1):1–13. https://doi.org/10.13225/j.cnki.jccs.2017.4400

Shi LQ, Qiu M, Wang Y, Qu XY, Liu TH (2019a) Evaluation of water inrush from underlying aquifers by using a modified water-inrush coefficient model and water-inrush index model: a case study in Feicheng coalfield, China. Hydrogel J 27:2105–2119. https://doi.org/10.1007/s10040-019-01985-2

Shi XZ, Zhu SY, Zhang WQ (2019b) Study on the mechanisms and prevention of water inrush events in a deeply buried high-pressure coal seam-a case study of the Chensilou Coal Mine in China. Arab J Geosci 12:614. https://doi.org/10.1007/s12517-019-4824-z

State Bureau of Coal Industry (2000) Regulations of pillar set and mining of building, water body, railway and main well lane. China Coal Industry Publishing House, Beijing

Sun WJ, Zhou WF, Jiao J (2016) Hydrogeological classification and water inrush accidents in China's coal mines. Mine Water Environ 35:214–220. https://doi.org/10.1007/s10230-015-0363-3

Wang H, Dong SN, Chai R, Liu QS (2015) Technical status of mine water control in china and its development strategy. Springer International Publishing, Cham

Wu LY, Bai HB, Yuan C, Wu GM, Xu CY, Du Y (2019) A water-rock coupled model for fault water inrush: a case study in Xiaochang coal mine. China Adan Civil Eng. https://doi.org/10.1155/2019/9343917

Yin SX, Wang Y, Yin HC, Xu B, Wang TJ, Yang JW, Tian WZ, Xu W, Cao M (2020) Mechanism and full-time-space prevention and control technology of water inrush from Ordovician and thin limestone in deep mines. J China Coal Soc 45(5):1855–1864. https://doi.org/10.13225/j.cnki.jccs.2020.0398

Zhang X (2011) Study on mechanism of slurry diffusion and sealing at the process of underground engineering moving water grouting and its application. Shandong University, Jinan

Zhang JC, Zhang YZ (1997) Rock seepage and water inrush from coal seam floor. Geological Publishing House, Beijing

Zheng Z, Li SC, Liu RT, Zhu GX, Zhang LZ, Pan D (2015) Analysis of coupling effect between grout and rock mass during jointed rock grouting. Chin J Rock Mech Eng 24(S2):4054–4063. https://doi.org/10.13722/j.cnki.jrme.2015.0975